Journal of Radioanalytical and Nuclear Chemistry

Rapid measurements of ^{235}U fission product isotope ratios using an online, high-pressure ion chromatography inductively coupled plasma mass spectrometry protocol with comparison to isotopic depletion models

Emilie K. Fenske [A, B], Benjamin D. Roach[A,1], David C. Glasgow[A], Ralph H. Ilgner[A], Joseph M. Giaquinto[A]

[A]Oak Ridge National Laboratory, 1 Bethel Valley Road, Oak Ridge, TN, 37830, USA.

[B] Institute for Nuclear Security, University of Tennessee, 1640 Cumberland Avenue, Knoxville, TN, 37996, USA.

[1]Corresponding author: roachbd@ornl.gov

Rapid measurements of ^{235}U fission product isotope ratios with online high-pressure ion chromatography inductively coupled plasma mass spectrometry protocol and comparison to isotopic depletion models

Emilie K. Fenske [A, B], Benjamin D. Roach[A], David C. Glasgow[A], Ralph H. Ilgner[A], Joseph M. Giaquinto[A]

[A]*Oak Ridge National Laboratory, 1 Bethel Valley Road, Oak Ridge, TN, 37830, USA.*

[B] *Institute for Nuclear Security, University of Tennessee, 1640 Cumberland Avenue, Knoxville, TN, 37996, USA.*

Abstract

An automated online separation–direct analysis method, RAPID (Rapid Analysis of Post-Irradiation Debris), has been developed for the measurement of the concentration and isotopic composition of over 40 elements down to the low-picogram level. Here we discuss the application of RAPID to irradiated highly-enriched uranium, demonstrating that it has the sensitivity required to achieve precise, low-level analyses of non-natural isotopes, even in the presence of a bulk uranium matrix. Isotopic ratios have been successfully measured at the low-picogram level, and the accuracy of these ratios was confirmed using an isotopic depletion and decay modeling software to within 1–2%.

Keywords

Ion chromatography, inductively coupled plasma mass spectrometry, irradiation, rapid isotope analysis, nuclear material

Introduction

Rapid radiochemical analysis of fission products is a key element in the advancement of nuclear research and development, specifically in the areas of modeling and simulation, nuclear forensics, and isotope production [1, 2]. In the case of a nuclear event, for example, timely nuclear forensic analysis of the subsequent material is critical in the attribution process that will follow [3]; similarly, improvement of modeling capabilities

occurs through verification of fission products formed during reactor operation [4–8] and material irradiation [9, 10]. Notably, the well-characterized ^{235}U thermal fission products vary from stable isotopes to those with various lengths of half-lives (typically deemed short-lived, long-lived, etc.) [11, 12], thus, both radiometric and mass-based analyses are traditionally utilized. Regardless, to adequately and efficiently characterize the short-lived isotopes at the same time as the longer-lived and stable isotopes, an inclusive, rapid analytical method would prove beneficial.

Current analytical capabilities for short-lived fission products in these situations traditionally consist of radio-analytical techniques, mainly non-destructive gamma-ray spectroscopy [13–15], including neutron activation analysis [16]. Since these methods rely on detecting radiation emitted from nuclear materials, spectral interferences and the need for background discrimination can increase uncertainties and detection limits [17, 18]. However, high-pressure ion chromatography (HPIC), when combined with an inductively coupled plasma mass spectrometer (ICPMS), can separate elements of interest from interferences in addition to quantifying low-level masses in nuclear materials [19–22].

HPIC-ICPMS enables the separation and direct analysis of trace-level quantities of elements from various matrices, such as environmental samples, nuclear waste, and uranium ore. Almon [23] et al. introduced the procedure of analyzing fission products and actinides in nuclear waste using HPIC directly coupled to ICPMS (HPIC-ICPMS) beginning in 1991. In the early 2000's, HPIC-ICPMS methods were developed to analyze actinides, lanthanides, and other metals in samples such as "urban road dust" and atmospheric particles [24], environmental samples [25, 26], uranium materials [19], and spent nuclear fuel [27–31]. More recently, work has been done to isolate and determine the concentrations of elements such as Np [32], Mg [33], Sr [34, 35], Cs [36], Pu [37, 38], Nd [39], Bk/Cf [40], Sm [41], and various other metals [42, 43] from subsequent interferences and matrices in each sample.

The online separation-direct analysis method developed at Oak Ridge National Laboratory (ORNL), RAPID (Rapid Analysis of Post-Irradiation Debris), can complete a full isotopic analysis of over 40 elements, post dissolution, in less than one hour per sample. Previous work utilizing RAPID reported the stability and sensitivity of the method together with its robustness to a silicon-based, surrogate soil matrix, and a NIST Montana II soil standard, SRM-2711a [44–46].

The focus of this work is the application of RAPID, a hyphenated HPIC-ICPMS protocol that elementally separates and directly detects isotopes, to irradiated nuclear material, specifically highly-enriched uranium (HEU), to measure the isotopic compositions of the resultant fission elements without the requirement for lengthy, column based, chemical separations. The accuracy of these results is confirmed through comparison

to fission product yields generated by decay modeling software developed at ORNL, the Oak Ridge Isotope Generation (ORIGEN) code [47]. The current work further develops the RAPID method with the goal to achieve measurements of non-natural isotopic signatures, *i.e.* those of a fission-based origin, at concentrations ranging from those in spent fuels to those likely present in post-detonation material [48, 49].

Materials and Methods

Facilities and capabilities

The Nuclear Analytical Chemical and Isotopics Laboratory (NACIL) group at ORNL possesses the unique capability to handle samples containing curie levels of radioactivity in addition to cleanroom spaces for handling a wide range of radioactive sample types. Radiological containment capabilities include hot cells, gloveboxes, and C-zoned fume hoods.

NACIL also contains ORNL's Neutron Activation Analysis (NAA) laboratory, located within the High Flux Isotope Reactor (HFIR) facility. The HFIR is the highest flux (reactor-based) neutron source for research in the United States, operating at a consistent 85 MW [50]. NACIL's NAA laboratory is an irradiation facility with an average obtained flux of ~10^{14} n cm^{-2} s^{-1} of thermal neutrons. Its capabilities include a remote-handling cubicle and a decay station in the HFIR pool. The model utilized for this research accurately reproduces the flux spectrum within the specific pneumatic tube used for irradiation, thus enabling accurate prediction of total fissions in each sample.

Software and Data Processing

The SCALE code system [51], which was developed and is maintained by ORNL, is used internationally in support of spent nuclear fuel transportation and storage applications. SCALE includes an isotopic depletion and decay analysis module known as ORIGEN. In this work, the ORIGEN module in the SCALE code system is used to predict fission in irradiated HEU targets. All data reported references the isotopic peak areas determined by the Thermo Fisher Scientific Qtegra software, using an m/z trace and a pre-determined elution time. Peak fitting and smoothing were applied post-acquisition, enabling peak area comparisons between isotope peaks of the same element in a single run, yielding the atom percent isotopic ratios. The chromatographic peak fitting and smoothing values applied to determine peak area, found within the "Peak Detection" settings of the Qtegra software, are as detailed previously [44–46].

Method Precision and Bias

The precision, bias, and limit of detection of the method is very dependent on the element, it's elution time from the HPIC column, and sensitivity to ionization in the ICPMS plasma. The elution times, measurement precision, limits of detection, and signal stability have been detailed previously for 48 elements of interest to the nuclear fuels cycle [46]. In short, for the lanthanides, the determined limits of detection were in the low picogram-high femtogram scale, although in subsequent studies this is likely to be much lower, and very dependent on contamination. Isotope ratios at the high femtogram level were consistently measured to within 2% uncertainty, with a mass bias of 1-1.5% per mass unit difference between the isotopes measured.

Instrumentation

The equipment employed was a Thermo Scientific™ Dionex™ ICS-5000+ HPIC system coupled to a Thermo Scientific iCAP™ Q quadrupole ICP-MS. Chromatographic separation was performed using a metal-free HPIC pump ICS 5000 (ThermoFisher Scientific), an injection valve, an IonPac CG5A guard column, an IonPac CS5A column, and a thermal compartment, set at 35 ºC for consistent elution times and improved day-to-day reproducibility. Chosen for its dual functionality, the CS5A column has both cation and anion exchange sites, using both sulfonic acid and alkanol quaternary ammonium functional groups. The analytical column was connected to the nebulizer of the ICP-MS instrument using 20-cm-long PEEK tubing via a mixing T-piece. Nitric acid (HNO_3, 1.25M, ~5%) was pumped in to the mixing T-piece at 0.1 mL/min to acidify the sample post-column prior to nebulization. The iCAP was fitted with a cyclonic quartz spray chamber, a nickel sampler cone, and a nickel skimmer cone with a standard skimmer insert. A pre-defined daily QC performance report was used to ensure continued optimized iCAP operating conditions. The coupled instruments are housed in a radiological fume hood, enabling the analyses of highly-radioactive samples. The method development, isotopic detection limits, system stability, and elution profiles have been reported previously [46]. Table 1 summarizes the experimental and operating conditions of the HPIC-ICPMS system.

Table 1 Experimental and operating conditions of the HIPC-ICPMS system.

Thermo Scientific Dionex ICS-5000+ HPIC	
PEEK injection loop	50 µL
IonPac CG5A column	50 x 4 mm i.d.
IonPac CS5A column	250 x 4 mm i.d. Substrate 9 µm particles 40 µequivalents/column

Eluent flow rate	1.0 mL. min^{-1}
System pressure at 1.0 mL. min^{-1} Post-column 1.25M HNO_3 flow rate	~1600 psi 0.1 mL. min^{-1}
PEEK HPIC-ICPMS connection tubing	0.25 mm i.d.
Thermo Scientific iCAP Q quadrupole ICP-MS	
Sampler cone diameter	1.1 mm
Skimmer cone diameter	0.5 mm
Plasma power	1550 W
Interface temperature	35.0 °C
Nebulizer gas flow rate	1.0 l/min
Axillary gas flow rate	0.78 l/min
Cool gas flow rate	13.95 l/min

Reagents and standards

Eluents for HPIC and all other solutions were prepared with trace-metals basis grade chemicals and ultra-pure water (18.2 MΩ cm) from a Millipore Milli-Q™ water purification system. Chemicals for eluents include: diglycolic acid (DGA, $C_4H_6O_5$, recrystallized, Acros Organics, New Jersey, USA), 2,6-pyridinedicarboxylic acid (PDCA, $C_7H_5NO_4$, 99.999% metals basis, Fluka, Sigma-Aldrich Co.), glacial acetic acid ($C_2H_4O_2$, 99.99% trace metals basis, Sigma-Aldrich Co., 3050 Spruce Street, St. Louis, MO 63103 USA), and oxalic acid ($C_2H_2O_4$, 99.999% trace metals basis, Sigma-Aldrich Co.). These were dissolved in ultra-pure water, then buffered with ammonium hydroxide (NH_4OH, 20-22% as NH_3, trace metal grade, Fisher Scientific, 1 Reagent Lane, Fair Lawn, NJ 07410), to a final pH of 4.5 - 4.8. Eluent compositions were: 6 mM PDCA (with 90 mM acetic acid, buffered to pH 4.5); 100 mM oxalic acid (buffered to pH 4.8) and 100 mM DGA (buffered to pH 4.8).

Material irradiation and sample preparation

Two HEU targets were prepared by evaporating portions of New Brunswick Laboratory certified reference standard U930-D (93.2% ^{235}U) into high-purity silica ampoules (Figure 1). After flame-sealing, the ampoules were counted on high-purity germanium (HPGe) detectors to quantify the fissile mass. Following the guidance of the Los Alamos National Laboratory PAssive Non-Destructive Assay (PANDA) manual [52], the 185.7 keV gamma ray was analyzed in background-subtracted spectra. The activity determined was divided by the specific activity of ^{235}U (79.8 kBq/g) to yield the mass. The subsequent mass values were 30 ± 3.5 µg and 80

± 5 µg for Targets 1 and 2, respectively. An approximate ORIGEN calculation resulted in an irradiation time for the larger target of 48.5 minutes to reach roughly 1×10^{14} fissions.

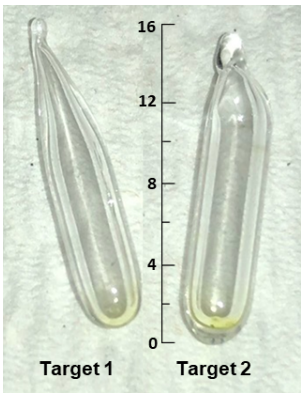

Fig. 1 Sealed targets of New Brunswick Laboratory certified reference standard U930-D (93.2% 235U) in high-purity silica ampoules. Inset: scale in mm.

On the day of irradiation, the thermal and epithermal flux populations were measured using dilute manganese and gold flux monitors, respectively. The thermal flux was 4.31×10^{14} and the epithermal measured 1.09×10^{13}, with both having units of neutrons cm^{-2} s^{-1}. For modeling purposes, the total flux over the broader neutron spectrum was calculated to be 6.69×10^{14} n cm^{-2} s^{-1}. The two targets were sealed in the same graphite rabbit and co-irradiated to ensure very similar neutron fluence. The irradiation lasted 48.5 minutes and the dose rate of the unopened rabbit was measured 24 hours post-irradiation totaling 1 Rem/h contact and about 40 mRem/h at 30 cm. After a 15-day cooling period, both irradiated targets were shipped from the HFIR facility to another NACIL laboratory building for chemical processing and analysis. The received targets were leached, while sealed, in 4M HNO_3, and tare weights in Savillex leaching vessels were determined. The targets were opened by submersion in 4M HNO_3 in a pre-leached, malleable polytetrafluoroethylene (PTFE) vessel under controlled crushing with a pre-cleaned mini-vice. The opened targets were then quantitatively transferred back into the pre-tared leaching vessels for sealed heat leaching. The vessels were heated to ~80°C for 4 h, allowed to cool, and the final weight was taken to determine solution weight and volume.

To ensure complete sample dissolution, the ^{235}U content was determined for each leached target using ICP-MS. The samples were externally calibrated, and a semi-quantitative analysis using two independent lots of a certified ^{238}U standard (IV-ICPMS-71A, Inorganic Ventures) was performed. The determined ^{235}U content was 27.4 ± 2.7 µg and 77.0 ± 3.9 total for Targets 1 and 2, respectively, well within the uncertainty of the 30 ± 3.5 and 80 ± 5 µg total ^{235}U determined via HPGe analysis prior to irradiation.

Results and discussion

Fission product analysis of irradiated HEU

36.1 days post-irradiation, fifty microliters of a 2× dilution (in 0.5M HNO_3) of each of the irradiated ^{235}U leachates (each target was leached into 3 mL of 4M HNO_3) was analyzed for fission product isotopic content, focusing on the lanthanide elements, as well as cesium, strontium, and ruthenium. The sensitivity of the method, shown in previous work [46], demonstrated that the lanthanide isotopic detection limit is in the high femtogram–low picogram scale. Due to this sensitivity, systematic natural contamination and background natural lanthanide content in the initial ^{235}U material (pre-irradiation) are measurable. Table 2 shows the measured lanthanide atom percent ratios compared to those calculated for natural isotopic abundance. The atom percent ratio recoveries confirmed that the lanthanides present in the U930-D material were of natural origin.

Table 2 Measured stable isotopic lanthanide atom % ratios in the U930-D material compared with natural data**

Ratio	Measured atom % ratio*	Natural atom % ratio**	Recovery
$^{140}Ce/^{142}Ce$	8.015	7.958	101%
$^{144}Nd/^{146}Nd$	1.389	1.384	100%
$^{147}Sm/^{152}Sm$	0.568	0.56	101%
$^{151}Eu/^{153}Eu$	0.927	0.916	101%
$^{157}Gd/^{158}Gd$	0.63	0.635	99%

*a natural mixed elemental standard is used to correct for mass bias, see also Precision and Bias section.

** All isotopic data was sourced from the National Nuclear Data Center [53].

Post irradiation, it was observed that cerium and neodymium were among the more contaminated lanthanides; however, information for each of the fission isotopes was still discernable. Among the lanthanides detected were: lanthanum, cerium, praseodymium, neodymium, promethium, and samarium (see Figure 2), which were all predicted to have thermal neutron-induced fission isotopes within a measurable range by the 36.1-day ORIGEN-calculated fission abundances (see Figure 3).

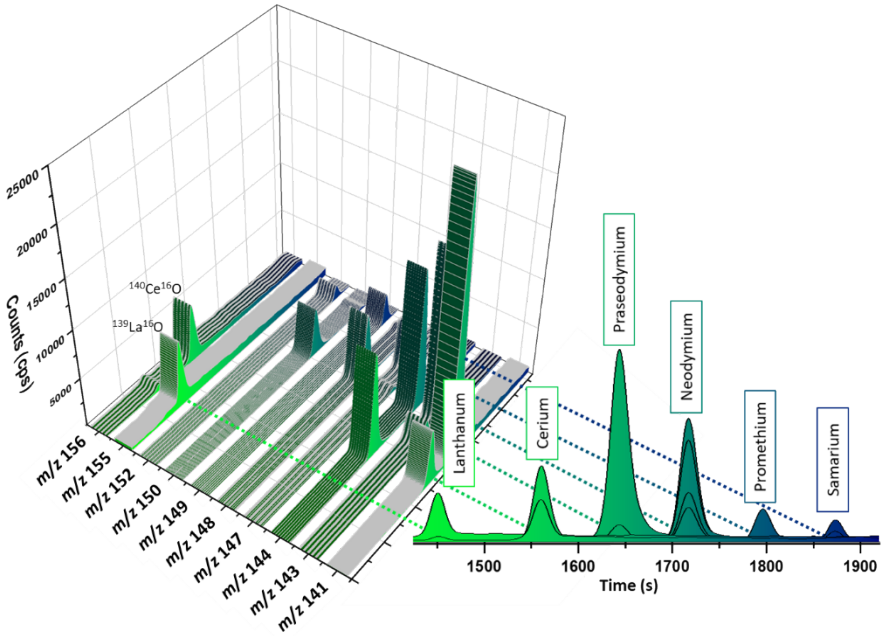

Fig. 2 3D staggered chromatograms of the m/z range 141-156, showing separation and various isotopes of the lanthanide series, with cerium, neodymium, and samarium isotopes bisected for clarity. Inset: a 2D layered chart showing the various isotopes observed at each elution time, where the largest observed species is labeled.

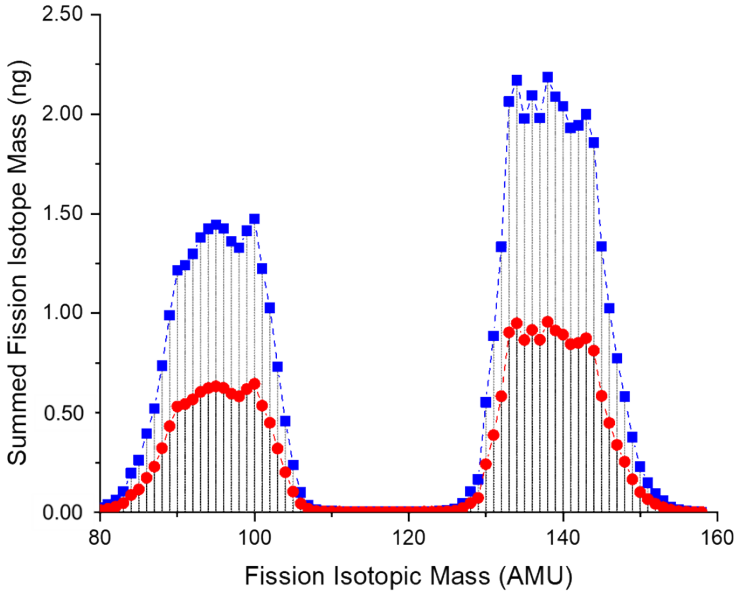

Fig. 3 ORIGEN calculation for Target 1 (red circles) and Target 2 (blue squares) for a 48.5-minute irradiation period, yielding approximately 1×10^{14} fissions**.** The graph shows the total fission quantity for each m/z (isotopes with the same m/z have been summed) after a 36.1 d decay period.

For all fission elements measured, a shift in the elution times was noted, relative to those previously observed (see Table 3) [46]. Nevertheless, this is unsurprising, as a significant amount of uranium is injected onto the column and may affect the column's retention efficacy. Other potential causes for the shift in elution times include: the acid concentration of the sample injected not the HPIC column, and slight changes in the pH of the buffered eluents.

Table 3 Elemental elution times for the lanthanide elements from the HEU matrix when compared to those reported previously* in various matrices [46].

Element	*Original elution time (s)	*Elution time in surrogate soil (s)	Elution time in irradiated HEU (s)
Cesium	165	190	230
Strontium	447	450	800
Ruthenium	130/400	100/350	165/380
Lanthanum	N/A	1,473	1,450
Cerium	1,675	1,600	1,560
Praseodymium	1,795	1,692	1,645
Neodymium	1,862	1,760	1,720
Samarium	1,990	1,830	1,865

Separation of the 147 m/z trace and determination of ^{147}Nd, ^{147}Pm, and ^{147}Sm

One noteworthy finding was the clear separation of the 147 masses: ^{147}Nd, ^{147}Pm, and ^{147}Sm. Figure 4 shows partial chromatograms of the m/z 147 trace, from Target 1 (dotted line) and Target 2 (solid line), showing the separation of the 147 isotopes. As mentioned earlier, the levels of natural lanthanide contamination have been seen to vary, and the ^{147}Sm concentration in Target 1 is larger than in Target 2; nonetheless, the separation enabled the determination of the ^{147}Nd/^{147}Pm atom percent ratios of 0.112 and 0.115 for Targets 1 and 2, respectively. With the ORIGEN-predicted atom percent ratio at the time of analysis being 0.116, the ratio recoveries were 97.0% and 99.5% for Targets 1 and 2, despite the injected isotopic mass of ^{147}Nd being only ~200 fg and ~600 fg onto the column.

$$^{147}\text{Nd}\ (t_{1/2} = 11\text{d}, \beta\text{-}) \rightarrow {}^{147}\text{Pm}\ (t_{1/2} = 2.6\text{y}, \beta\text{-}) \rightarrow {}^{147}\text{Sm} \qquad (1)$$

^{147}Nd decays to ^{147}Pm with a measurable decay energy of 896 keV; on the other hand, the decay of ^{147}Pm to stable ^{147}Sm emits only a weak gamma-ray at 121 keV, with an intensity of 0.00285% (see Eq. 1). Both the weak gamma and beta emissions are likely not measurable within any uncertainty in a "real-world" sample via radiochemical techniques. However, when coupled with a semi-quantitative analysis, using a ^{147}Sm tracer in a National Institute of Standards and Technology (NIST) tracible standard, it should be possible to determine the ^{147}Pm concentration to within a 5–10% uncertainty down to the low picogram–high femtogram level. It has been determined using the RAPID method that each of the lanthanide elements have a very similar response, with the integrated ^{159}Tb signal being only 5% larger than that observed for ^{139}La, despite a 20 AMU mass difference. With that obsevation, together with the excellent recovery of the ^{147}Nd/^{147}Pm atom percent ratios, it can be assumed that promethium shouldn't deviate from this trend. A natural samarium standard would be the most suitable isotope for a semi-quantitative analysis as it has a natrually occuring *m/z* 147 isotope and is directly adjacent to promethium in the periodic table, with very similar 1st ionization potentials (5.582 and 5.643 eV for promethium and samarium respectively) [REF].

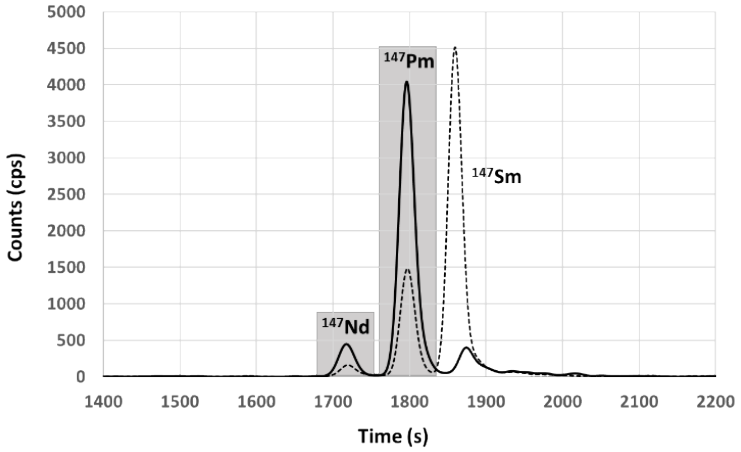

Fig. 4 Partial chromatograms of the m/z 147 from Target 1 (dotted line) and Target 2 (solid line), showing clear separation of 147 masses of Nd, Pm, and Sm.

Measuring the isotopes of neodymium

The isotopes of neodymium are among the more prominent in the ORIGEN-calculated fission masses. The neodymium isotopic composition measured for both targets, although consistent, matches neither the predicted fission nor a natural abundance: they appear to be a mixture of both. This is to be expected, as the uranium source material was already determined to be contaminated with natural neodymium. In order to determine the isotopic composition of the neodymium produced in fission, the determined isotopic composition must be corrected. There are two ways in which a correction can be made, where the first is through use of ^{147}Nd, a

uniquely fission-based isotope, and the ORIGEN-predicted fission abundance. The second would be to correct the isotopic composition for natural contamination using the ^{142}Nd isotope, an isotope not produced in fission [54]. Table 4 lists the natural abundance and ORIGEN-predicted fission abundance of the neodymium isotopes, in addition to the isotopic abundances observed for each target. Using the measured ^{142}Nd, the natural neodymium contamination was calculated to be 68 and 66 % for Targets 1 and 2, respectively. By using ^{147}Nd, the fission neodymium was determined to be 36 and 34 % for Targets 1 and 2, respectively, confirming the ^{142}Nd-based values. The determined atom percent abundances due to neutron-induced fission, which are the measured values, for both targets were corrected for natural abundances determined prior to the neutron irradiation. The averaged corrected values with a 2σ standard deviation, also given in Table 4, match the ORIGEN-predicted values within the uncertainty of the measurement.

Table 4 The normalized natural abundance and ORIGEN-predicted fission atom % abundance of the measured Nd isotopes, and the normalized isotopic atom % abundances observed for each target.

Isotope	Natural abundance (atom %)	Fission Abundance (atom %, calc.)	Target 1 (atom %, meas.)*	Target 2 (atom %, meas.)*	Average fission atom % (corr.) (2σ)**
^{142}Nd	27.15	**0.00**	18.0	17.8	**0.0**
^{143}Nd	12.17	33.08	20.0	20.1	33.2(1)
^{144}Nd	23.80	3.11	16.1	15.9	3.0(1)
^{145}Nd	8.29	26.45	14.6	15.0	26.3(8)
^{146}Nd	17.19	20.16	17.6	18.3	19.5(17)
^{147}Nd	**0.00**	1.55	0.6	0.5	1.6(2)
^{148}Nd	5.76	11.26	8.0	7.5	11.7(14)
^{150}Nd	5.64	4.39	5.0	4.8	4.7(7)

Note: *mass bias correction applied using a natural neodymium standard. ^{147}Nd mass bias interpolated using a linear regression curve of the other isotopes. ** corrected for natural abundances, determined prior to the neutron irradiation. All Nd isotopes in table are stable or primordial, but the short-lived ^{147}Nd (11 day half-life).

Measuring cerium isotopes produced by thermal neutron fission

Similar to neodymium, several isotopes of cerium are also prominent in the calculated fission masses. However, the natural contamination of cerium is significant with the two stable isotopes ^{140}Ce and ^{142}Ce being

at least an order of magnitude larger than the mass of fission cerium present. Two non-natural isotopes have been measured and compared with the ratio predicted by ORIGEN. ^{141}Ce (32.5 d, β decay to ^{141}Pr) and ^{144}Ce (284.9 d, β decay to ^{144}Pr; 16 min, β decay to ^{144}Nd) were measured in both targets. Figure 5 shows the m/z 141 and m/z 144 chromatograms, illustrating clear separation between the cerium isotopes (t = 1560 s) and the ^{141}Pr and ^{144}Nd isobaric interferences (seen at t = 1640 s and 1720 s, respectively).

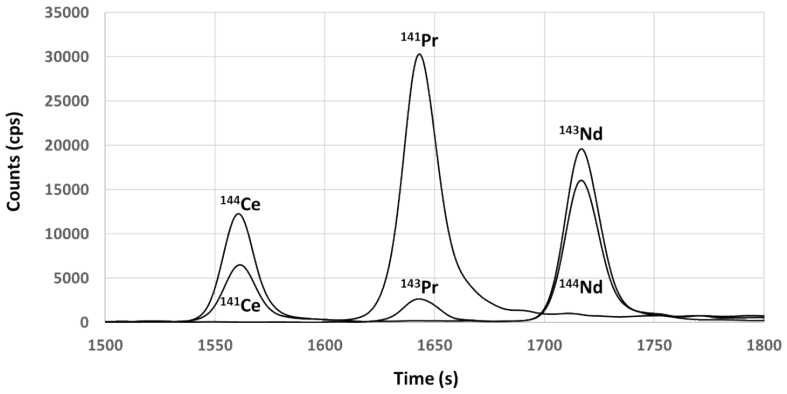

Fig. 5 The 141 m/z, and 144 m/z chromatograms for Target 2, showing the ^{141}Ce and ^{144}Ce peaks (t=1560 s) and the isobaric interferences ^{141}Pr (t=1640 s) and ^{144}Nd (t=1740 s). Also shown is the 143 m/z chromatogram for elemental confirmation of the Nd and Pr.

When the observed ^{141}Ce :^{144}Ce ratios for Targets 1 and 2 (see Table 5) are compared with the ORIGEN ratio calculated with a 36.1 d decay time post-irradiation, the recoveries are 98 and 99% for Targets 1 and 2, respectively.

Table 5 The observed ^{141}Ce:^{144}Ce atom % ratios for Targets 1 and 2 with the ORIGEN atom % ratio calculated with a 36.1-day decay time post-irradiation.

Target	Observed ^{141}Ce:^{144}Ce	Calculated ^{141}Ce:^{144}Ce	^{141}Ce:^{144}Ce % recovery
1	0.516	0.528	98
2	0.523	0.528	99

Measuring non-natural samarium isotope ratios produced by thermal neutron fission

As observed for the other lanthanides thus far, natural samarium was found as a contaminant in the dissolved targets. Target 1 was shown to have significant samarium contamination, which meant isotopic data was not useful. Target 2, however, showed little natural contamination, and the primary non-natural samarium isotope

produced in fission (bar ^{153}Sm, which at the time of analysis had decayed beyond detection due to its short half-life of 46h), ^{151}Sm ($t_{1/2}$ = 90 y), could be used to elucidate sample information.

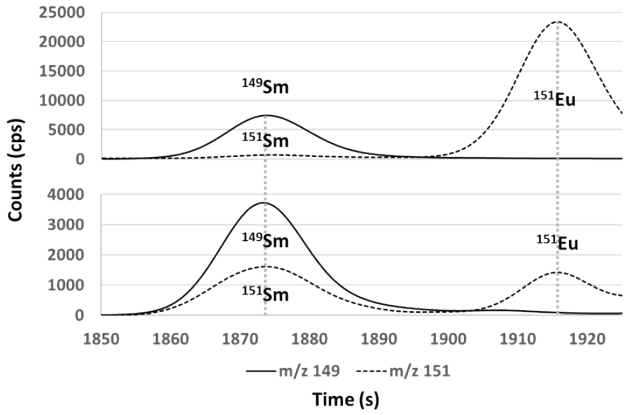

Fig. 6 The 149 m/z and 151 m/z chromatograms, showing separation of the ^{151}Sm (t=1875 s) from the isobaric contaminant ^{151}Eu isotope (t=1920 s) in Target 1 (top panel) and Target 2 (bottom panel)

Figure 6 displays the m/z 149 and m/z 151 chromatograms, showing the ^{151}Sm (t = 1875 s) and the contaminant ^{151}Eu isotope (t = 1920 s) peaks. Target 1 (Figure 6, top panel) shows significant natural samarium and europium contamination. The observed ^{149}Sm :^{151}Sm ratio for Target 2 showed 99% recovery when compared with that calculated (2.53 vs 2.55). Although, as other calculated ratios do not show as good a recovery, this may just be coincidental and driven primarily by the high fission abundances of both isotopes.

Measuring cesium isotopes produced by thermal neutron fission

There also appears to be natural contamination of ^{133}Cs in the leached targets (calculated to be 15% and 2% in targets 1 and 2 respectively), which affects the recoveries of the cesium isotopic composition when compared with those predicted by ORIGEN. However, as seen with cerium, cesium has two non-natural isotopes that can be measured and compared with the predicted ratio, ^{135}Cs and ^{137}Cs. ^{135}Cs has an extremely long half-life (2.3×10^6 y) and is difficult to measure using gamma spectroscopy at the levels predicted by ORIGEN, and natural barium (^{135}Ba, 6.6% natural abundance, ^{137}Ba, 11.2% natural abundance), present in almost all-natural samples of glass and soil, will likely mask the ^{135}Cs and ^{137}Cs content when traditional mass spectrometry methods are used. Figure 7 shows the baseline-corrected m/z 133, m/z 135, and m/z 137 chromatograms for Target 2, showing separation from the naturally-occurring barium isotopes (t = 90 s, and 280 s). The barium content is three to four orders of magnitude larger than the cesium content and shows significant peak tailing; despite this, the peak picking software uses each of the individual m/z baselines to determine peak area. When the observed ^{135}Cs/^{137}Cs ratios for Targets 1 and 2 (see Table 6) are compared with the ORIGEN ratio

calculated with a 36.1 d decay time post-irradiation, the recoveries are 102% and 99% for Targets 1 and 2, respectively.

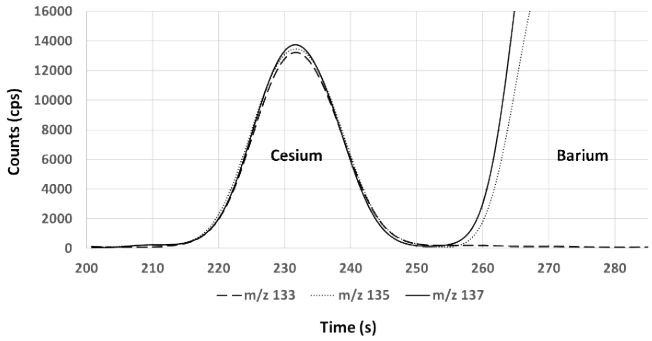

Fig. 7 Baseline corrected 133, 135, and 137 m/z chromatograms for Target 2, showing clear separation between the naturally-occurring barium isotopes ^{135}Ba and ^{137}Ba (t=90 s) and cesium.

Table 6 Observed cesium isotopic compositions and ^{135}Cs:^{137}Cs ratios for Targets 1 and 2, compared with the ORIGEN ratio calculated with a 36.1-day decay time post-irradiation.

Target	^{133}Cs atom (%)	^{135}Cs atom (%)	^{137}Cs atom (%)	^{135}Cs:^{137}Cs ORIGEN	^{135}Cs:^{137}Cs measured	% Recovery
1	43.2	28.7	28.2	0.999	1.018	102
2	33.1	33.5	33.9	0.999	0.987	99

Measuring ruthenium isotopes produced by thermal neutron fission

Measuring the ruthenium isotopic ratio ^{101}Ru:^{102}Ru demonstrated the sensitivity of the method down to the calculated isotopic LODs (4 pg injection for Target 1) [46]. Figure 8 displays the m/z 101 and m/z 102 chromatograms for Targets 1 and 2. Even with both peak areas being at the detection limit for the method, the ^{101}Ru:^{102}Ru ratio was measured at 1.05 and 1.20 (1.19 calculated by ORIGEN, 85% and 101% recovery). Target 1 exhibited ^{101}Ru and ^{102}Ru peak areas at barely five times background, and the error associated with it reflected the observed ^{101}Ru:^{102}Ru ratio of 1.05 (85% recovery).

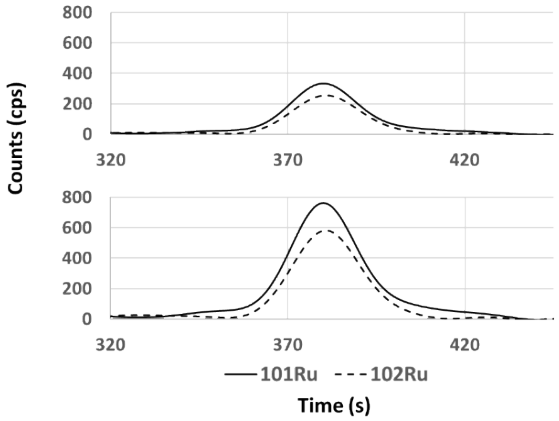

Fig. 8 The 101 and 102 m/z chromatograms for Target 1 (above) and Target 2 (below), showing the ^{101}Ru and ^{102}Ru peaks.

Measuring strontium isotopes produced by thermal neutron fission

Similar to ruthenium, when measuring the isotopic ratio ^{89}Sr:^{90}Sr, the accuracy and sensitivity of the method is observed at the calculated isotopic LODs (5 pg injection of ^{89}Sr for Target 2) [46]. Figure 9 shows the m/z 89 and m/z 90 chromatograms for Target 2: with both peak areas being at the detection limit for the method, the recovery of the ^{89}Sr:^{90}Sr ratio for both targets was still 93% (0.46 vs 0.49 as calculated by ORIGEN). The lower recovery is likely due to mass bias effects that have been shown to be more prominent in the lower mass range; this is particularly the case for strontium [55]. To address this, a low-level natural strontium standard could be employed as a mass bias standard using the ^{86}Sr:^{87}Sr ratio.

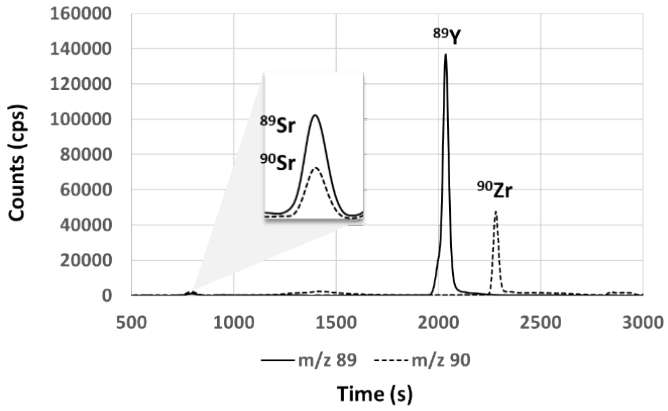

Fig. 9 The 89 and 90 m/z chromatograms for Target 2, showing the ^{89}Sr and ^{90}Sr peaks.

Summary of determined fission isotopic ratios

As can be seen from the summary of determined isotopic ratios for fission products in Targets 1 and 2, provided in Table 7, this modified HPIC-ICPMS method can measure isotopic ratios to within as little as 1% of that predicted by ORIGEN. Target 2, being 2.3× larger in mass, yielded higher fission isotopic masses, which is reflected in the accuracies associated with the subsequent isotopic ratios. Of note, N/A denotes that sample contamination prevented analysis or both isotopes measured fell below the LOD.

Table 7 Summary of measured isotopic ratios with their recovery from that calculated in ORIGEN.

Element	ORIGEN calculated ratio	Measured ratio in Target 1 (% recovery)	Measured ratio in Target 2 (% recovery)
^{135}Cs:^{137}Cs	0.999	1.018 (102)	0.987 (99)
^{89}Sr:^{90}Sr	0.49	N/A	0.46 (93)
^{101}Ru:^{102}Ru	1.19	1.05 (85)	1.20 (101)
^{141}Ce:^{144}Ce	0.528	0.516 (98)	0.523 (99)
^{147}Nd:^{147}Pm	0.116	0.112 (97)	0.115 (100)
^{149}Sm:^{151}Sm	2.55	N/A	2.53 (99)

Conclusions

The work presented here built on previous work by extending the RAPID method to elements of non-natural isotopic abundances in a uranium matrix. After leaching of the irradiated HEU targets, the isotopic ratios of several key fission elements, namely cesium, strontium, ruthenium, lanthanum, cerium, praseodymium, neodymium, promethium, and samarium, were investigated. Most of the fission isotope ratios investigated presented a 1–2% difference between measured and an ORIGEN model, even with analyzed masses being in the sub-picogram range. Overall, the uranium matrix appeared to have little effect on the sensitivity or reproducibility of the method, although the elution times of some of the monitored fission products were slightly shifted.

With the low detection limits and high robustness to matrices, this method could potentially provide a valuable tool for the nuclear research and development community. The speed with which the method can be remotely performed is beneficial not only to reduce the dose to the operator, but also to significantly reduce the analysis time. However, although very promising, this study is preliminary and only isotope ratio accuracy when compared to ORIGEN models has been reported.

Future Work

Understanding the RAPID method limitations in the presence of a uranium matrix was a key part to future studies both in a soil- and actinide-based matrix. Further investigations include the application of isotope

dilution mass spectrometry for high precision fission isotopic concentration measurements, the incorporation of both a silicon and a uranium matrix, measurement of irradiated material after a much shorter cooling time, varying irradiation times and neutron flux, and the application of the method to an irradiated ^{239}Pu-based material. Once the method has been established using well-characterized isotopes, we also plan on extending the application to lesser characterized and modeled isotopes, such as ^{237}Np, which is of interest at ORNL, as it is the target isotope used for the production of ^{238}Pu.

Acknowledgement

This submission has been authored by a contractor of the U.S. Government under contract No. DE AC05-00OR22725. Accordingly, the U.S. Government retains a non-exclusive, royalty-free license to publish or reproduce the published form of this contribution, or allow others to do so, for the U.S. Government purposes. This work was sponsored by the Defense Threat Reduction Agency (DTRA).

This manuscript has been authored in part by UT-Battelle, LLC, under contract DE-AC05-00OR22725 with the US Department of Energy (DOE). The US government retains and the publisher, by accepting the article for publication, acknowledges that the US government retains a nonexclusive, paid-up, irrevocable, worldwide license to publish or reproduce the published form of this manuscript, or allow others to do so, for US government purposes. DOE will provide public access to these results of federally sponsored research in accordance with the DOE Public Access Plan (http://energy.gov/downloads/doe-public-access-plan). This research was supported in part by an appointment to the Oak Ridge National Laboratory Post-Master's Research Associate Program, sponsored by the U.S. Department of Energy and administered by the Oak Ridge Institute for Science and Education.

References

1. Hofmann S (2003) Chapter 1: Properties and Syntheses of Superheavy Elements. In: Schädel M (ed) The Chemistry of Superheavy Elements. Kluwer Academic Publishers, pp 1–27

2. Roberto JB, Alexander CW, Boll RA, et al (2015) Actinide targets for the synthesis of super-heavy elements. Nucl Phys A 944:99–116 . doi: 10.1016/j.nuclphysa.2015.06.009

3. Keegan E, Kristo MJ, Toole K, et al (2016) Nuclear Forensics: Scientific Analysis Supporting Law Enforcement and Nuclear Security Investigations. Anal Chem 88:1496–1505 . doi: 10.1021/acs.analchem.5b02915

4. Gauld IC, Giaquinto JM, Delashmitt JS, et al (2016) Re-evaluation of spent nuclear fuel assay data for the Three Mile Island unit 1 reactor and application to code validation. Ann Nucl Energy 87:267–281 . doi: 10.1016/j.anucene.2015.08.026

5. Ilas G, Gauld IC, Radulescu G (2012) Validation of new depletion capabilities and ENDF/B-VII data libraries in SCALE. Ann Nucl Energy 46:43–55 . doi: 10.1016/j.anucene.2012.03.012

6. Cantrel L, Cousin F, Bosland L, et al (2014) ASTEC V2 severe accident integral code: Fission product modelling and validation. Nucl Eng Des 272:195–206 . doi: 10.1016/j.nucengdes.2014.01.011

7. Tait JC, Gauld I, Kerr AH (1995) Validation of the ORIGEN-S code for predicting radionuclide inventories in used CANDU fuel. J Nucl Mater 223:109–121 . doi: 10.1016/0022-3115(94)00683-0

8. Casoli P, Authier N, Laurec J, et al (2012) Measurements of Actinide-Fission Product Yields in Caliban and Prospero Metallic Core Reactor Fission-Neutron Fields. J ASTM Int 9:104018 . doi: 10.1520/JAI104018

9. Chadwick MB, Kawano T, Barr DW, et al (2010) Fission Product Yields from Fission Spectrum n+239Pu for ENDF/B-VII.1. Nucl Data Sheets 111:2923–2964 . doi: 10.1016/j.nds.2010.11.003

10. Shinohara N, Kohno N, Nakahara Y, et al (2003) Validation of Minor Actinide Cross Sections by Studying Samples Irradiated for 492 Days at the Dounreay Prototype Fast Reactor—I: Radiochemical Analysis. Nucl Sci Eng 144:115–128 . doi: 10.13182/NSE03-A2347

11. Bolles RC, Ballou NE (1959) Calculated Activities and Abundances of U235 Fission Products. Nucl Sci Eng 5:156–185 . doi: 10.13182/NSE59-A25574

12. Tipnis S V., Campbell JM, Couchell GP, et al (1998) Yields of short-lived fission products produced following 235U thermal neutron fission. Phys Rev C 58:905–915 . doi: 10.1103/PhysRevC.58.905

13. Metz LA, Payne RF, Friese JI, et al (2009) Experimental measurements of short-lived fission products from uranium, neptunium, plutonium and americium. J Radioanal Nucl Chem 282:373–377 . doi: 10.1007/s10967-009-0225-1

14. Dayman K, Biegalski S, Haas D (2015) Determination of short-lived fission product yields with gamma spectrometry. J Radioanal Nucl Chem 305:213–223 . doi: 10.1007/s10967-015-3993-9

15. Finn EC, Metz L, Greenwood L, et al (2015) Cumulative fission yields of short-lived isotopes under natural-abundance-boron-carbide-moderated neutron spectrum. J Radioanal Nucl Chem 306:79–91 . doi: 10.1007/s10967-015-4085-6

16. Knowles J, Skutnik S, Glasgow D, Kapsimalis R (2016) A generalized method for characterization of 235U and 239Pu content using short-lived fission product gamma spectroscopy. Nucl Instruments Methods Phys Res Sect A Accel Spectrometers, Detect Assoc Equip 833:38–44 . doi: 10.1016/j.nima.2016.06.112

17. Tshiashala MDA (2005) Instrumental neutron activation analysis in geochemistry: Emphasis on spectral and uranium fission product interferences. J Radioanal Nucl Chem 265:511–514 . doi: 10.1007/s10967-005-0857-8

18. Landsberger S, Simsons A (1987) Quantification of uranium, thorium and gadolinium spectral interferences in instrumental neutron activation analysis of samarium. Chem Geol 62:223–226 . doi: 10.1016/0009-2541(87)90087-8

19. Röllin S, Kopatjtic Z, Wernli B, Magyar B (1996) Determination of Lanthanides and Actinides in Uranium Materials by High-Performance Liquid Chromatography with Inductively Coupled Plasma Mass Spectrometry. 739:139–149

20. Epov V, Evans R, Zheng J, et al (2007) Rapid fingerprinting of 239 Pu and 240 Pu in environmental samples with high U levels using on-line ion chromatography coupled with high-sensitivity quadrupole ICP-MS detection. J Anal Atom Spectrom 22:1131–1137 . doi: 10.1039/B704901C

21. Hann S, Prohaska T, Köllensperger G, et al (2000) Separation of spectral and non-spectral interferences by on-line high performance ion chromatography inductively coupled plasma sector field mass spectrometry (HPIC-ICP-SFMS) for accurate determination of 234U, 235U, 238U and 232Th in industrial ores. J Anal Atom Spectrom 15:721–725 . doi: 10.1039/B001076F

22. Bürger S, Riciputi LR, Bostick DA, et al (2009) Isotope ratio analysis of actinides, fission products, and geolocators by high-efficiency multi-collector thermal ionization mass spectrometry. Int J Mass Spectrom 286:70–82 . doi: 10.1016/j.ijms.2009.06.010

23. Almon AC, Kinard WF, Dewberry RA, et al (1991) Multimodal Separation of Alkali, Alkaline Earth, Transition, Post-Transition, Lanthanide, and Actinide Metal Cations in Waste Sludge (U)

24. Bruzzoniti MC, Cavalli S, Mangia A, et al (2003) Ion chromatography with inductively coupled plasma mass spectrometry, a powerful analytical tool for complex matrices Estimation of Pt and Pd in environmental samples. J Chromatogr A 997:51–63 . doi: 10.1016/S0021-9673(03)00547-8

25. Epov V, Lariviere D, Reiber K, et al (2004) Extraction and determination of Cs in natural waters by ICP-MS after ion exchange separation. J Anal Atom Spectrom 19:1225–1229 . doi: 10.1039/B403013C

26. Betti M, Menichetti L, Moreno JM, Fuoco R (2000) A preliminary study for the determination of long-lived radionuclides (second transition group 4-d) in environmental samples by ion chromatography inductively coupled plasma-mass spectrometry (IC-ICP-MS). Microchem J 67:285–290 . doi: 10.1016/S0026-265X(00)00074-6

27. Betti M (1997) Use of ion chromatography for the determination of fission products and actinides in nuclear applications. J Chromatogr A 789:369–379 . doi: 10.1016/S0021-9673(97)00784-X

28. Smith M, Farmer O, Reeves J, Koppenaal D (1995) Radionuclide detection by ion-chromatography and on-line ICP/MS and beta detection: Fission product rare earth element measurements. J Radioanal Nucl Chem Artic 194:7–13 . doi: 10.1007/BF02037607

29. Alonso JIG, Sena F, Arbore P, et al (1995) Determination of fission products and actinides in spent nuclear fuels by isotope dilution ion chromatography inductively coupled plasma mass spectrometry. J Anal At Spectrom 10:381 . doi: 10.1039/ja9951000381

30. Röllin S, Eklund UB, Spahiu K (2001) Separation of actinide redox species with cation exchange chromatography and its application to the analysis of spent fuel leaching solutions. 89:757–763

31. Wolf SF, Bowers DL, Cunnane JC (2005) Analysis of high burnup spent nuclear fuel by ICP-MS. 263:581–586

32. Snow M, Morrison S, Clark S, et al (2017) 237Np analytical method using 239Np tracers and application to a contaminated nuclear disposal facility. J Env Radioact 172:89–95 . doi: 10.1016/j.jenvrad.2017.02.018

33. Karasinski J, Bulska E, Wojciechowski M, et al (2017) High precision direct analysis of magnesium isotope ratio by ion chromatography/multicollector-ICPMS using wet and dry plasma conditions. Talanta 165:64–68 . doi: 10.1016/j.talanta.2016.12.033

34. García-Ruiz S, Moldovan M, García Alonso JI (2008) Measurement of strontium isotope ratios by MC-ICP-MS after on-line Rb-Sr ion chromatography separation. J Anal At Spectrom 23:84–93 . doi: 10.1039/b708936h

35. Karasinski J, Bulska E, Wojciechowski M, et al (2016) On-line separation of strontium from a matrix and determination of the 87 Sr/ 86 Sr ratio by Ion Chromatography/Multicollector-ICPMS. J Anal Atom Spectrom 31:1459–1463 . doi: 10.1039/C6JA00109B

36. Yang G, Tazoe H, Yamada M (2016) Rapid determination of 135Cs and precise 135Cs/137Cs atomic ratio in environmental samples by single-column chromatography coupled to triple-quadrupole inductively coupled plasma-mass spectrometry. Anal Chim Acta 908:177–184 . doi: 10.1016/j.aca.2015.12.041

37. Puzas A, Genys P, Remeikis V, Druteikienė R (2015) Challenges in preparing soil samples and performing a reliable plutonium isotopic analysis by ICP-MS. J Radioanal Nucl Ch 303:751–759 . doi: 10.1007/s10967-014-3411-8

38. Liao H, Zheng J, Wu F, et al (2008) Determination of plutonium isotopes in freshwater lake sediments by sector-field ICP-MS after separation using ion-exchange chromatography. Appl Radiat Isot 66:1138–1145 . doi: 10.1016/j.apradiso.2008.01.001

39. Guéguen F, Isnard H, Nonell A, et al (2014) Neodymium isotope ratio measurements by LC-MC-ICPMS for nuclear applications: investigation of isotopic fractionation and mass bias correction. J Anal Atom Spectrom 30:443–452 . doi: 10.1039/C4JA00361F

40. Gourgiotis A, Isnard H, Nonell A, et al (2013) Bk and Cf chromatographic separation and 249Bk/248Cm and 249Cf/248Cm elemental ratios determination by inductively coupled plasma quadrupole mass spectrometry. Talanta 106:39–44 . doi: 10.1016/j.talanta.2012.11.056

41. Bourgeois M, Isnard H, Gourgiotis A, et al (2011) Sm isotope composition and Sm/Eu ratio determination in an irradiated 15 Eu sample by ion exchange chromatography -quadrupole inductively coupled plasma mass spectrometry combined with double spike isotope dilution technique. J Anal Atom Spectrom 26:1660–1666 . doi: 10.1039/C1JA10070J

42. Michalski R, Jabłonska M, Szopa S, et al (2011) Application of Ion Chromatography with ICP-MS or MS Detection to the Determination of Selected Halides and Metal/Metalloids Species. Crit Rev Anal

Chem 41:133–150 . doi: 10.1080/10408347.2011.559438

43. Winter C, Seubert A (2016) Usability of online-coupling ion exchange chromatography ICP-AES/-MS for the determination of trivalent metal complex species under acidic conditions. J Anal At Spectrom 31:1262–1268 . doi: 10.1039/c5ja00480b

44. Roach BD, Hexel CR, Giaquinto JM (2017) ORNL TM-2017-694: Demonstration of a Rapid HPLC-ICPMS Direct Coupling Technique Using IDMS Project Report Part I

45. Roach BD, Glasgow DC, Fenske EK, et al (2017) ORNL TM-2017-697: Demonstration of a Rapid HPLC-ICPMS Direct Coupling Technique Using IDMS Project Report Part II

46. Roach BD, Fenske EK, Ilgner RH, et al (2017) RAPID: Development of a fast and efficient analytical technique for the isotopic analysis of fission and actinide elements in environmental matrices. J Chromatogr A (accepted)

47. Gauld IC, Radulescu G, Ilas G, et al (2011) Isotopic Depletion and Decay Methods and Analysis Capabilities in SCALE. Nucl Technol 174:169–195 . doi: 10.13182/NT11-3

48. Eppich G, Knight K, Timothy J-H, et al (2014) Constraints on fallout melt glass formation from a near-surface nuclear test. J Radioanal Nucl Ch 302:593–609 . doi: 10.1007/s10967-014-3293-9

49. Hanson S, Pollington A, Waidmann C, et al (2016) Measurements of extinct fission products in nuclear bomb debris: Determination of the yield of the Trinity nuclear test 70 y later. Proc Natl Acad Sci 113:8104–8108 . doi: 10.1073/pnas.1602792113

50. ORNL High Flux Isotope Reactor. https://neutrons.ornl.gov/hfir

51. Rearden, BT Oak Ridge National Laboratory SCALE Website

52. Reilly D, Ensslin N, Smith Jr H, Kreiner S (1991) Passive Nondestructive Assay of Nuclear Materials. United States Nuclear Regulatory Commission

53. Laboratory BN National Nuclear Data Center. http://www.nndc.bnl.gov/

54. Rider BF, Ruiz C., Peterson Jr. JP, Smith FR (1967) Determination of neodymium-148 in irradiated uranium and plutonium as a measure of burnup

55. Meija J (2012) Calibration of isotope amount ratios by analysis of isotope mixtures. Anal Bioanal Chem 403:2071–2076 . doi: 10.1007/s00216-012-5785-1